Nanostructured liquid crystalline particles as delivery vectors for isofuranodiene: Characterization and in-vitro anticancer activity

Nanostructured Liquid Crystalline Particles as Delivery Vectors for Isofuranodiene: Characterization and *In-vitro* Anticancer Activity

Michela Pisani,[a] Luana Quassinti,[b] Massimo Bramucci,[b] Rossana Galassi,[c] Filippo Maggi,[b] Barbara Rossi,[d] Alessandro Damin,[e] Patricia Carloni,[f] Paola Astolfi[a*]

[a] Department of Science and Engineering of Materials, Environment and Urban Planning - SIMAU, Marche Polythecnic University, Via Brecce Bianche 12, I- 60131 Ancona, Italy

[b] School of Pharmacy, University of Camerino, I-62032 Camerino, Italy

[c] School of Science and Technology, Chemistry Division, University of Camerino, Via Sant'Agostino 1, I-62032 Camerino, Italy

[d] Elettra - Synchrotron Trieste S.C.p.A., S.S. 14 - km 163.5, I-34149 Basovizza, Trieste, Italy

[e] Department of Chemistry, NIS Centre and INSTM Reference Centre University of Turin, Via G. Quarello 15, I-10135 Turin, Italy

[f] Department of Agricultural, Food and Environmental Sciences - D3A, Marche Polythecnic University, Via Brecce Bianche, I- 60131 Ancona, Italy

[*] Corresponding author: e-mail p.astolfi@univpm.it; phone +39-071-2204416

Authors: e-mail m.pisani@univpm.it, massimo.bramucci@unicam.it; luana.quassinti@unicam.it; rossana.galassi@unicam.it; filippo.maggi@unicam.it; barbara.rossi@elettra.eu; alessandro.damin@unito.it; p.carloni@univpm.it

Abstract

Isofuranodiene is an oxygenated sesquiterpene containing a furan ring isolated from the essential oil of *Smyrnium olusatrum* L. (Apiaceae) owning notable anticancer activity. Despite its biological potential, the high lipophilicity along with a relatively low stability due to Cope rearrangement giving rise to a less active compound, make the perspective of its therapeutical use unlikely. On this basis, in the present work we evaluated bulk and dispersed non lamellar liquid crystalline phases as effective delivery vectors for isofuranodiene, and capable of preserving its structure and enhancing the biological activity. Small-angle X-ray scattering, dynamic light scattering, and UV resonance Raman spectroscopy were used to characterize the nanosystems in an integrated experimental approach. Encapsulation of isofuranodiene in the lipid matrix resulted in a transition from a cubic *Im3m* to a

reversed hexagonal phase because of the highly lipophilic character of the drug, as obtained in SAXS measurements, and in significant shifts in the components of the Raman spectrum of isofuranodiene. The anticancer activity of isofuranodiene-loaded lipidic nanoparticles was assessed on MDA-MB 231 cell line by MTT assay and was found to be higher than that of pristine isofuranodiene.

Keywords

Cubic and Hexagonal Liquid Crystals, Cubosomes, Hexosomes, Isofuranodiene, Glyceryl Monooleate

Abbreviations

GMO, Glyceryl monooleate; F127, Pluronic® F127; IFD, Isofuranodiene; SAXS, Small-Angle X Ray Scattering; UVRR, UV Resonant Raman; CI, Combination Index

1. Introduction

Bioactive compounds obtained from natural sources have been extensively used through the centuries from different traditional medicines.[1] Their choice is dictated by many reasons ranging from the fact that their assumption is better psychologically accepted to the opinion they are considered less toxic than the artificial analogues.[2] Many extracts, essential oils and compounds isolated from plants are very active and currently used for several therapeutics purposes.[3] Thereby, the extraction of active compounds from plants and the research on their pharmacological benefits and on their possible pharmaceutical formulations represent a very rich field of research and stimulus for new and sustainable economies.[4,5,6] Isofuranodiene (IFD, syn. furanodiene) is a lipophilic sesquiterpene isolated from plant species of the genera *Commiphora*,[7] *Curcuma*,[8] *Eugenia*[9] and *Smyrnium*;[10,11] some of these have a long history and their earlier uses are dated back to the eastern alternative medicine, in the traditional Chinese medicine and in Ayurveda. IFD has several potential therapeutic effects ranging from multiple anticancer activities,[10,12,13,14,15] to antitripanosomal,[16] anti-inflammatory[17] and hepatoprotective effects.[18,19,20] It follows that there is a continuous interest in the therapeutic effects and in the mechanism of actions of this molecule,[19,21,22,23] as such and as a co-drug,[24] and in its possible use in clinical trials. IFD, once isolated in the solid state, may undergo a thermal conversion (Cope rearrangement) to curzerene, a less active compound.[25] Pharmaceutical formulations for IFD delivery[26] are hence considered with the aim to preserve its integrity and to enhance its solubility and bioavailability. In fact, the sesquiterpene IFD is a non-polar molecule with a very low water solubility and a net positive value for logP of 3.52,[27] and its dispersion in a lipid matrix represents a plausible route for its stabilization and delivery.[28,29] About this issue, a pioneer study was published by Zhang et *al*. in 2017,[27] where IFD was loaded in folate-mediated PEGylated nanostructured lipid carriers

FA-PEG$_{2000}$-DSPE-NCLs to increase its solubility and bioavailability, prolong the circulation time in blood and improve the targeting ability. Other systems were tested to encapsulate IFD or its rich essential oils such as PLGA Biodegradable PolyLactide-co-Glycolide nanoparticles,[30] or as water-dispersible SNEDDS (self-nano-emulsifying drug delivery system) formulation and microemulsions.[31,32] Lipid dispersions may also be obtained from amphiphiles having a hydrophilic headgroup and a hydrophobic chain region which self-assemble upon addition of water to form a series of liquid crystalline structures ordered in one, two and three dimensions. Upon addition of water amphiphiles may self-assemble into lyotropic liquid crystalline systems (LLC) with the hydrophobic moieties clustering together to minimize the exposure to water and the hydrophilic moieties oriented to the water environment. Lamellar (L_α), hexagonal (H) and bicontinuous cubic (Q) phases, according to their symmetry, are the most commonly studied.[33] In particular, the hexagonal and the cubic mesophases can be classified in "normal" (type I) with hydrocarbon domains embedded in a continuous water medium (oil-in-water systems), and "inverted" (type II) with the polar headgroups, hydrated by water, organized in a continuous non polar matrix (water-in-oil systems).[34] In the inverted hexagonal phase (H_{II}), the structural cylindrical elements are filled with water and dispersed in a continuous medium formed by the hydrocarbon chains, whereas the polar headgroups are at the water/hydrocarbon interface.[35] Inverted bicontinuous cubic phases consist of a complex 3-D lipid bilayer wrapped around two intertwined and unconnected water networks. [36] They can exist in three different space groups: double gyroid *Ia3d*, double diamond *Pn3m* and primitive *Im3m*. LLC phases are not very easy to handle because of their viscosity,[37] but this may be reduced by adding a steric stabilizer and dispersing these materials into nanoparticles whose internal structures closely resemble that of the parent bulk liquid crystal phase. Once dispersed, the H_{II} and Q_{II} phases are termed hexosomes and cubosomes, respectively and in recent years they are attracting considerable interest as potential nano-carriers for both hydrophilic and hydrophobic drugs,[38,39] vitamins,[40] as well as for proteins and nucleic acids.[41,42] Different amphiphiles are currently used but most of the LLC research concerns glyceryl monooleate GMO[43,44] or phytantriol PHYT,[45] which, in the presence of a water excess, self-assemble in a bicontinuous cubic phase. Both compounds are promising for cosmetic[46] and medical[47] applications as they are included in the FDA inactive ingredients guide. Recently, phytantriol was employed, alone or in combination with a cationic surfactant,[48,49] to encapsulate the anticancer agent 5-fluorouracil and the systems were characterized by different complementary techniques-. The same integrated experimental approach (characterization by small-angle X-ray scattering, UV resonance Raman spectroscopy and dynamic light scattering) was used in the present work to analyse GMO lipid matrices which were loaded, for the first time, with isofuranodiene in order to preserve its structure and to enhance its biological activity. At this regard, GMO/IFD

colloidal dispersions were tested for their *in vitro* anticancer potential using human MDA-MB-231 cancerous cells as model.

2. Materials and methods

2.1 Materials

Glyceryl monooleate (GMO) (Monomuls® 90-O18) was a gift from BASF, Germany. It has a similar composition to other commercial GMO-based products with phases behaviour like that of the pure component.[43] Isofuranodiene (IFD) was isolated from the essential oil obtained from the inflorescences of *Smyrnium olusatrum* L. by crystallization following a previously reported procedure.[50,26] Its chemical structure was confirmed by NMR analysis by comparison with literature and reference standard available in authors' laboratory.[25,51] Pluronic® F127 (PEO_{98}-PPO_{67}-PEO_{98}) was a Sigma-Aldrich products. Milli-Q water was used for the hydration of the lipids and for all the dilutions. Chloroform and methanol were obtained from Sigma-Aldrich; they were of analytical grade and used as received.

2.2 Preparation of Bulk Lipid Phases

GMO (50 mg) and Pluronic® F127 (8 % w/w of lipid) were dissolved in chloroform and, after solvent evaporation, dried under vacuum. The residue was hydrated with water (200 μL) and equilibrated at room temperature for 24 hours to obtain the cubic phase gel.

The same procedure was used for IFD loaded cubic gels but adding 4 mg of IFD to GMO/F127 chloroform mixture before evaporation of the solvent.

2.3 Preparation of Dispersed Lipid Phases

Lipid dispersions were obtained upon addition of water to the gels (final lipid concentration 20 mg/mL) and 10 min probe sonication (pulse mode, 1s on and 1 s off, 50 % maximum power).

2.4 Small Angle X-Ray Scattering (SAXS)

Synchrotron SAXS measurements were performed at the SAXS beamline, Elettra Sincrotrone Trieste (Trieste, Italy). 2-Dimensions diffraction images were recorded on a Dectris Pilatus 1M detector at 1.54 Å wavelength (8keV incident beam energy). The sample to detector distance was 1279 mm which covers a q range of 0.15-5 nm^{-1} ($q = 4\pi \sin\theta / \lambda$ where λ is the wavelength and 2θ is the scattering angle). A vacuum chamber was arranged between the sample and the detector to remove the air scattering. Exposure time for each sample was set to 1 s. 1D intensity versus q patterns were obtained from the integration of the recorded 2D scattering images. From the linear fit of the plot q_{hkl}

vs $\sqrt{h^2 + k^2 + l^2}$ and q_{hkl} *vs* $\sqrt{h^2 + k^2 + hk}$ the lattice parameters a for the cubic and hexagonal phase were obtained, respectively.

2.5 UV Resonant Raman (UVRR)

UVRR experiments were carried out at the BL10.2-IUVS beamline of Elettra Sincrotrone Trieste (Italy).[52] The 228 nm exciting wavelength was selected by suitably regulating the undulator gap and using a Czerny-Turner monochromator (Acton SP2750, Princeton Instruments). A triple stage spectrometer (Trivista, Princeton Instruments), having a spectral resolution of ca. 15 cm^{-1}, was employed for collecting the spectra in a back-scattered geometry. Cyclohexane was used for the calibration of the spectrometer. The radiation power on the sample was ~10 μW. Any possible photo-damage effect following a prolonged UV-rays exposure of the sample was avoided by continuously spinning the sample cell during the measurements. In order to evidence the single spectral components in the experimental Raman profiles, a fitting procedure of the UVRR spectra was implemented by using a sum of a minimum number of Pseudo-Voigt functions. All the parameters were initialized with reasonable values and then they were gradually released up to the convergence of the fit.

Calculations were performed by adopting the Gaussian 09 software[53] and the pure exchange-correlation PBE[54] DFT based functional, including the D3-bj empirical dispersive term.[55] H atoms were described by a 6-31+G(d,p) standard Pople Gaussian basis set, C and O atoms by a 6-31+G(2d,p) one. Then the optimized isofuranodiene molecule was used for Raman spectrum calculation.

2.6 Particle Size and Zeta Potential

Dynamic light scattering measurements were performed to have the average particle size distribution (*PSD*) of the prepared aqueous dispersions, whereas electrophoretic light scattering to measure the Zeta Potential Zp of the nanoparticles. In both cases, a Malvern Zetasizer Nano ZS was employed. The *PSD* was characterized by polydispersity index (*PDI*) and Z-average values (Z_{ave}) for particle diameter. They were measured immediately after preparation (t = 0 days) as well as in the following 45 days to monitor the physical stability of the dispersions over time.

The obtained values are the means of measurements performed in triplicate on three different samples, properly diluted with water, at 25 °C assuming the viscosity of water. For data analysis, the Zetasizer software DTS V 7.10 was used.

2.7 IFD Content in Nanostructured GMO Dispersions

The IFD entrapment efficiency of the prepared hexosomes was determined as described previously[48] after separation of drug loaded hexosomes from excess IFD by centrifuging the IFD loaded nanoparticles at 10,000 rpm for 15 min by using centrifugal filter tubes with a 10 kDa cut-off (Amicon Ultra-4, Millipore). The collected filtrate was read at λ_{max} = 220 nm to eventually quantify the non-encapsulated IFD. Total IFD (free and encapsulated, *IFD(T)*) was determined at λ_{max} = 220 nm after addition of methanol to disrupt the lipid nanostructures.

Encapsulation efficiency *EE (%)* was obtained from the equation:

$$EE\ (\%) = \frac{IFD(T) - IFD(F)}{IFD(T)}\ x\ 100$$

where *IFD(T)* and *IFD(F)* are the total and the free IFD used in the preparation of hexosomes and collected in the filtrate, respectively.

Measurements were conducted in triplicate on three independent samples.

2.8 Cell culture.

Human breast adenocarcinoma cells (MDA-MB 231) were obtained from American Type Culture Collection (Rockville, MD) and maintained in Dulbecco's Modified Eagle's Medium (DMEM) with 2 mM L-glutamine, 100 IU/mL penicillin, 100 µg/mL streptomycin (Corning, Manassas, VA, USA), and supplemented with 10% heat-inactivated fetal bovine serum (HI-FBS) (Corning, Manassas, VA, USA). Cells were grown in a humidified atmosphere with 5% CO_2 at 37°C. Cells were maintained in culture by detachment with Tripsin/EDTA and diluted in fresh medium before reaching the cell confluence state (approximately 80% confluence).

2.9 Antiproliferative activity

The cytotoxic potential of GMO and GMO/IFD nanoparticles on MDA-MB 231 cell viability was investigated. The reduction of tetrazolium salt, 3-(4,5-dimethylthiazol-2-yl)-2,5-diphenyl-2H-tetrazolium bromide (MTT; Sigma-Aldrich, St. Louis, MO) to formazan by mitochondrial succinate dehydrogenase was used to evaluate the viability of the cancer cells as previously described.[56] Briefly, exponentially growing cells were seeded in quadruplicate at the density of 2×10^4 cells/mL into 96-well microtiter tissue culture plates (Corning Incorporated, NY, USA) in complete medium (100 µL) and incubated at 37 °C in a 5% CO_2 atmosphere. After 24 h from the seeding the cells in culture plates, GMO and GMO/IFD nanoparticles in appropriate concentrations were added. GMO and GMO/IFD nanoparticles were tested in the 6.3-400 µg lipid/mL concentration range, whereas bare IFD was tested in the 0.8-200 µg/mL range. Pluronic® F127 was also tested at the maximum concentration of 32 µg/mL corresponding to F127 concentration in the 400 µg/mL dispersion. After 24 and 48 h of incubation, cell viability was determined by adding 10 µL of MTT solution (5 mg/mL in phosphate-buffered saline, PBS) to each well. After 4 h additional incubation at 37 °C, the culture

medium was removed, and formazan crystals were dissolved in 100 µL of dimethyl sulfoxide (DMSO; Sigma-Aldrich). The plates were stirred for about 15 min in order to solubilize the crystals and the absorbance was read at λ = 540 nm Optical Density using an OMEGA plate reader from BMG Labtech (Durham, NC, USA). Experiments were conducted in triplicate. Cytotoxicity was expressed as the concentration of compound inhibiting cell growth by 50% (IC_{50}) relative to control cells.

2.10 Statistical analysis

Quantitative data were presented as means ± SD from three independent experiments. The significance of differences was evaluated with one-way ANOVA followed by Bonferroni multiple Comparison Test. The IC_{50} values and statistical analysis were executed with GraphPad Prism 5 Software (S. Diego, CA, USA) using $p \leq 0.05$ as the critical level of significance. The computer software, CompuSyn, was used to determine the effects (synergistic, additive or antagonistic) of GMO/IFD interactions at all doses and effect levels,[57] as indicated by the combination index (CI) obtained from the CI equation algorithms. A CI value less than 1 means that there is a synergic effect, a value of 1 indicates an additive effect and a value greater than 1 indicates an antagonistic effect.

3. Results

3.1 Characterization of Bulk Phases

The first step in the investigation was the assessment of the influence of IFD on GMO phase structure in excess of water. Since in the present work both the bulk and dispersed systems were used, samples were all prepared with the same composition by including the block copolymer F127. As reported in Table 1, an *Im3m* cubic phase with a lattice constant a = 13.40 nm was observed for the empty bulk cubic phase as confirmed by the X-ray diffraction pattern with the typical Bragg peaks (110), (200), (211), (310), (222) shown in Figure 1(a). No signals from other bicontinuos cubic phases were evident in the diffraction pattern, differently from what reported by other authors.[58,59] The incorporation of IFD into the GMO matrix led to a transition from an *Im3m* cubic to an H_{II} phase with unit dimension cell a = 6.30 nm (Figure 1(b)). This phase behaviour can be justified by considering the critical packing parameter (CCP, a shape factor)[60] defined as CPP = V/Al and can be estimated considering the amphiphile dimensions: V and l are the volume and the length of the hydrophobic part of the amphiphile, respectively whereas A is the cross-sectional area of the hydrophilic headgroup. For reverse structures CPP is typically larger than 1 and, in the present case, the addition of the lipophilic drug IFD in the lipid matrix should expand the volume of the hydrophobic moiety thus increasing the

CPP value and favouring the transition toward a more negatively curved mesophase such as the hexagonal one.

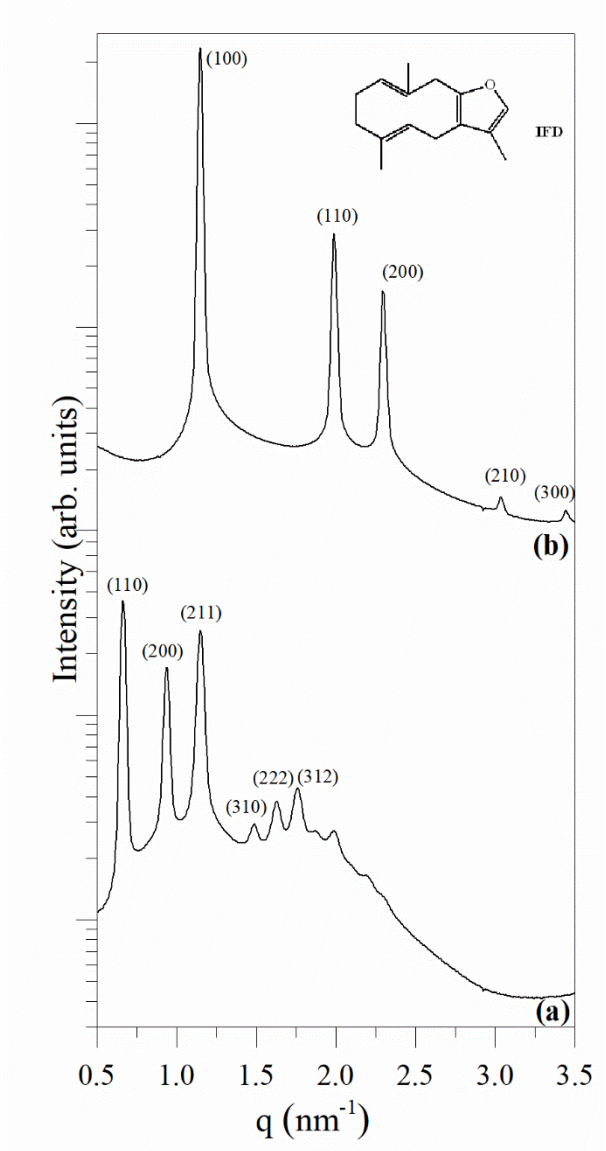

Figure 1. SAXS diffraction profiles of GMO bulk phase: unloaded, *Im3m* cubic phase (a) and IFD loaded, H_{II} hexagonal phase (b)

In Figure 2(a)-(b) the experimental Raman spectrum of pristine IFD molecule and the calculated Raman intensities in the 1300-1800 cm^{-1} region are compared. The experimental profile of Figure 2(a) shows the presence of three intense features that can be recognized at ≈1555, 1625 and 1670 cm^{-1}. By comparison between experimental and calculated Raman spectra, these spectral components can reasonably be associated to the corresponding calculated Raman frequencies at ≈1551, 1673 and 1686 cm^{-1}, respectively, that appear in the spectrum of Figure 2(b). As visualized by the sketches reported in the same panel of Figure 2(b), the experimental component at 1555 cm^{-1} (calculated at 1551 cm^{-1}) can be attributed to a stretching vibration of the IFD furan ring. Conversely, the Raman contributions found at ≈1625 and 1670 cm^{-1} in the experimental spectrum (calculated at 1673 and

1686 cm^{-1}) can be attributed to stretching movements mainly involving the double bonds located on the IFD condensed rings.

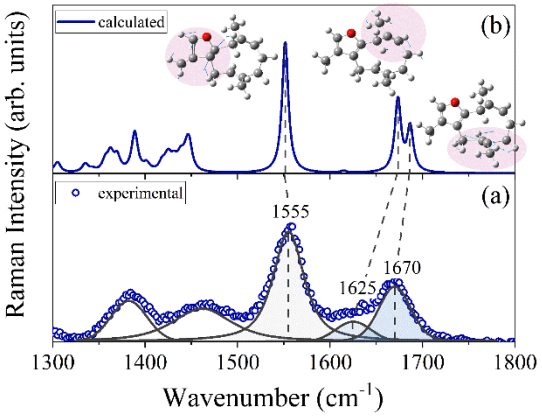

Figure 2. Experimental (a) and calculated Raman (b) spectrum of pristine IFD in the wavenumber region 1300-1800 cm^{-1}. The sketches reported in panel (a) visualizes the vibrational modes associated to the corresponding calculated frequencies and the coloured areas highlight the molecular moieties mainly involved in the vibration.

Figure 3(a)-(b) shows the UVRR spectra of IFD pristine and loaded in GMO matrix. The use of 228 nm exciting radiation for collecting Raman spectra allowed us to enhance the intensity of IFD Raman peaks between 1500 and 1800 cm^{-1} involving the aromatic moieties in the drug structure. Moreover, the use of exciting wavelength below 250 nm had the great advantage of strongly reducing the interfering fluorescence background that often affects the spontaneous Raman spectra of these organic compounds. The Raman profile of GMO matrix loaded with IFD is dominated by the signals arising from the drug while the less intense contribution of GMO has been easily subtracted from the total experimental profile reported in Figure 3(b). The comparison between the spectra of Figure 3(a) and (b) evidences some spectral changes undergone by IFD when it is loaded in GMO matrix, suggesting the existence of an interaction between the drug and GMO molecular group in the complex. Particularly, a significant red-shift of ≈10 cm^{-1} is observed for the IFD Raman component that in pristine form is found at about 1625 cm^{-1}. Small shifts are observed also for the other two contributions centred at ≈1555 and 1670 cm^{-1} in the pure drug, which slightly move at ≈1557 and 1666 cm^{-1} upon encapsulation in GMO. Additionally, the loading of IFD into GMO matrix clearly induces a change in the relative intensities of the three Raman components that are visible in the region 1500-1800 cm^{-1}. By considering these shifts and analysing the structures of both IFD and of GMO, we can argue two possible sites of interactions for these molecules: the oxygen atom of the furane ring and the polar head of the lipid matrix for an eventual dipole dipole attraction on the one side, and the long alkyl chain of the GMO and the dienyl ring of IFD, according to local polarizations,

on the other side. This last option fits with the observed C=C double bonds Raman shifts as polarization is supposedly more effective on the C=C double bonds. This is consistent with the resonance occurring for these functional groups at the excitation wavelength of 228 nm that leads to a major sensitivity of the UVRR technique also for slight spectral modifications involving C=C double bonds. All these experimental findings are consistent with the encapsulation inside GMO of IFD whose molecular groups are influenced by a more hydrophobic environment than the free drug.

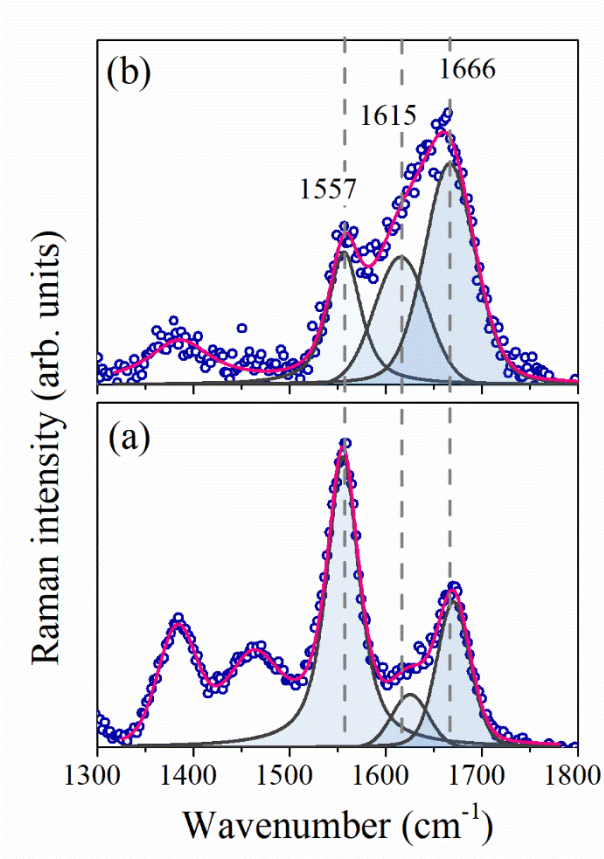

Figure 3. UVRR spectrum of IFD pristine (a) and loaded in GMO (b) in the wavenumber region 1300-1800 cm^{-1}. The total fit-curve and the single components assigned to Raman spectral components are represented with full lines.

3.2 Characterization of Dispersions

GMO and GMO/IFD nanoparticles were prepared by dispersion of the bulk cubic/hexagonal phases, already added of F127. The effectiveness of the steric stabilizer was confirmed by the homogeneous appearance of the dispersions. In fact, uniform milky mixtures with no signs of aggregation were obtained for both the empty and loaded samples, with the GMO dispersion a little less opaque than the GMO/IFD one.). The more or less opaque appearance of the dispersions depends by the scattering

of the visible component of the incident light, and is higher (more opaque sample) in case of the IFD loaded dispersion because of the higher nanoparticles average size and PDI (see Table 1)

The inner organization of the dispersed lipid NPs was determined, and both the phase structure and the lattice parameters were the same as the parent bulk phase. Empty dispersions were in a cubic *Im3m* mesophase (a = 13.40 nm), whereas the IFD loaded sample assumed an inverted hexagonal (H_{II}) type structure (a = 6.25 nm).

Dynamic light scattering (DLS) measurements indicated that both formulations have a monomodal size distribution (Table 1) with a mean particle size of 176 nm for GMO/IFD hexosomes larger than the Z_{ave} determined for the empty cubosomes (132 nm). The low PDI values indicate homogeneity of the formulations and stability of the cubic and hexagonal NPs against aggregation.

Table 1. Average particle size (Z_{ave}) and Polydispersity Index (PDI) of GMO nanoparticles, empty and loaded with IFD, measured for 45 days

	GMO		GMO/IFD	
days	**Z_{ave} (nm)**	**PDI**	**Z_{ave} (nm)**	**PDI**
0	132.10 ± 1.38	0.08 ± 0.01	175.90 ± 2.26	0.16 ± 0.03
7	135.61 ± 1.37	0.10 ± 0.03	198.20 ± 2.82	0.18 ± 0.03
14	136.94 ± 1.61	0.10 ± 0.01	200.10 ± 3.80	0.19 ± 0.05
21	137.27 ± 1.65	0.09 ± 0.02	203.70 ± 3.60	0.19 ± 0.04
28	137.73 ± 1.51	0.09 ± 0.01	200.80 ± 4.50	0.21 ± 0.04
45	138.47 ± 2.02	0.10 ± 0.02	198.30 ± 3.30	0.22 ± 0.02

The prepared dispersions have a good colloidal stability as indicated by the size and size distribution values monitored for a period of 45 days. Just a small increase in the particle size was observed in the first 7 days for the loaded nanoparticles and the PDI value varied little with time.

A Zeta Potential Zp value of -20.27 ± 0.95 mV was measured for GMO cubosomes, in agreement with the previous literature.[61] IFD encapsulation in the nanoparticles had no significant effect on the Zp, which slightly decreased to -24.24 ± 0.85 mV. Negative values were obtained for the formulations even if all the components, GMO, Pluronic® F127 and IFD, are uncharged. This behaviour may be connected to possible contamination of commercial GMO by free oleic acid which may be partially ionized or to the adsorption of hydroxyl ions,[62,63] coming from the aqueous environment, favoured from the coverage of the nanoparticle surface by the PEO groups of Pluronic® F127; in fact these PEO groups of F127 stretches out of the nanosystem acting as a corona.[61,64]

A good IFD entrapment efficiency in the nanoparticles (93.2 ± 4.7 %) was obtained and it can be attributed to the compatibility between the drug and the matrix: the lipid bilayers of these nanoparticles provide a suitable environment for this highly hydrophobic molecule (logP = 3.52).[27]

The *in vitro* anticancer activity of IFD-loaded GMO nanoparticles, and for comparison that of the bare IFD, were determined in human breast adenocarcinoma MDA-MB 231 cells and evaluated by MTT assay. In fact, IFD was found to be an antiproliferative agent towards human colon carcinoma,[13] prostate and breast cancer cells in vitro and to be less toxic in normal cells.[65,66] IFD was shown to inhibit MCF7 and MDA-MB 231 cells proliferation and to induce depolarization, chromatin condensation and DNA fragmentation. Moreover, it was found to increase the Bad and Bax expression, the proteolytic cleavage of caspase-9, caspase-7 and poly-ADP-ribose polymerase (PARP) and to inhibit the protein expression of cyclins, Rb, Bcl-xLand Akt in these cell lines.[65] The *in vitro* cytotoxicity of GMO nanoparticles was investigated on different cell lines,[67,68,69,70] but few and not very clear data are available on the effects of GMO on MDA-MB 231 cells.[71,72] In a previous work,[48] MDA-MB 231 cells were used to test the cytotoxicity of cubosomes, empty and loaded with 5-fluorouracil, but they were made of phytantriol. It was found that PHYT nanoparticles were not toxic for concentration up to 75 µg/mL after 24 h of incubation and that the toxicity drastically increased after 72 h. Here, the toxicity of GMO cubosomes on MDA-MB 231 cells was tested and it was found that they were found less toxic than PHYT cubosomes, in agreement with literature data collected on different cellular lines,[67] where GMO was found to have a lower ability to disrupt the cellular membrane. The IC_{50} values determined in this work were 116.9 and 127.4 µg/mL after 24 and 48 h of cells incubation in the presence of GMO, as reported in Table 2. Pluronic® F127, used as stabilizer, resulted non-toxic even at the highest used concentration (data not shown).

Table 2. Cytotoxic activity of IFD, GMO and GMO/IFD on MDA-MB 231cell line.

	MDA-MB 231 (IC_{50} µg/mL)	
	24 h	48 h
IFD	27.73	24.56
95% C.I.[a]	23.11 - 33.26	21.50 - 28.05
GMO	116.9	127.4
95% C.I.	100.8 - 135.6	120.1 - 135.1
GMO/IFD	79.9	92.7
95% C.I.	72.17 - 88.45	86.45 - 99.41

IC_{50} = The concentration of compound that reduces by 50% the cell growth (after 24 and 48 h of incubation).
[a] Confidence interval.

A low IFD concentration did not show any inhibition of MDA-MB 231 cell viability; instead, higher concentrations determine a dose-dependent decrease of viability (Fig. 4). As reported in Table 2, IC_{50} values for IFD were 27.73 and 24.56 µg/mL at 24 h and 48 h, respectively. To enhance solubility and bioavailability, IFD was encapsulated in GMO cubosomes with the incorporation ratio of 1.625 mg IFD/20 mg GMO and the nanoparticles obtained were used to test the antiproliferative activity of GMO/IFD complex on MDA-MB 231 cells. As reported in Table 2, IFD encapsulation in GMO nanoparticles resulted in a significantly enhanced anticancer activity of the loaded nanoparticles compared to the empty ones, being the IC_{50} values at 24 h 116.9 µg/mL and 79.9 µg/mL for the GMO and GMO/IFD, respectively The antiproliferative activity of the two systems at the different concentrations tested is shown in Figure 4 (a and b) for the 24 and 48 h treatment. For both the samples the concentrations refer to the lipid content, whereas the corresponding concentration of IFD in GMO/IFD is indicated in the upper axis of the diagram. Upon treatment with 100 µg/mL GMO or GMO/IFD, a reduction in cell viability from 68.9 % (GMO) to 35.7 % (GMO/IFD) at 24 h treatment was observed as shown in Figure 4 (a). In 100 µg/mL GMO/IFD 8.1 µg/mL IFD were encapsulated but, at this concentration, pristine IFD had almost no toxicity (Figure 4, panel c) and hence IFD loaded in the nanoparticles was more effective than the free drug. The complex had almost the same cytotoxic effect prolonging the incubation time to 48 h.

Noteworthy, cells incubated with GMO or GMO/IFD were treated with two different kinds of nanoparticles, cubosomes and hexosomes, respectively and this could result in a different cytotoxicity. Even if both the systems have the same concentration of monoolein and F127, the different internal structures and surface curvature of the two kind of nanoparticles may influence their interaction with the lipid membranes of cells, [73] making hexosomes less toxic than cubosomes. Other factors could account for the minor cytotoxicity of hexosomes, such as their higher elasticity and softness,[74] or their minor interfacial area which determines a minor amount of associated F127.[75]

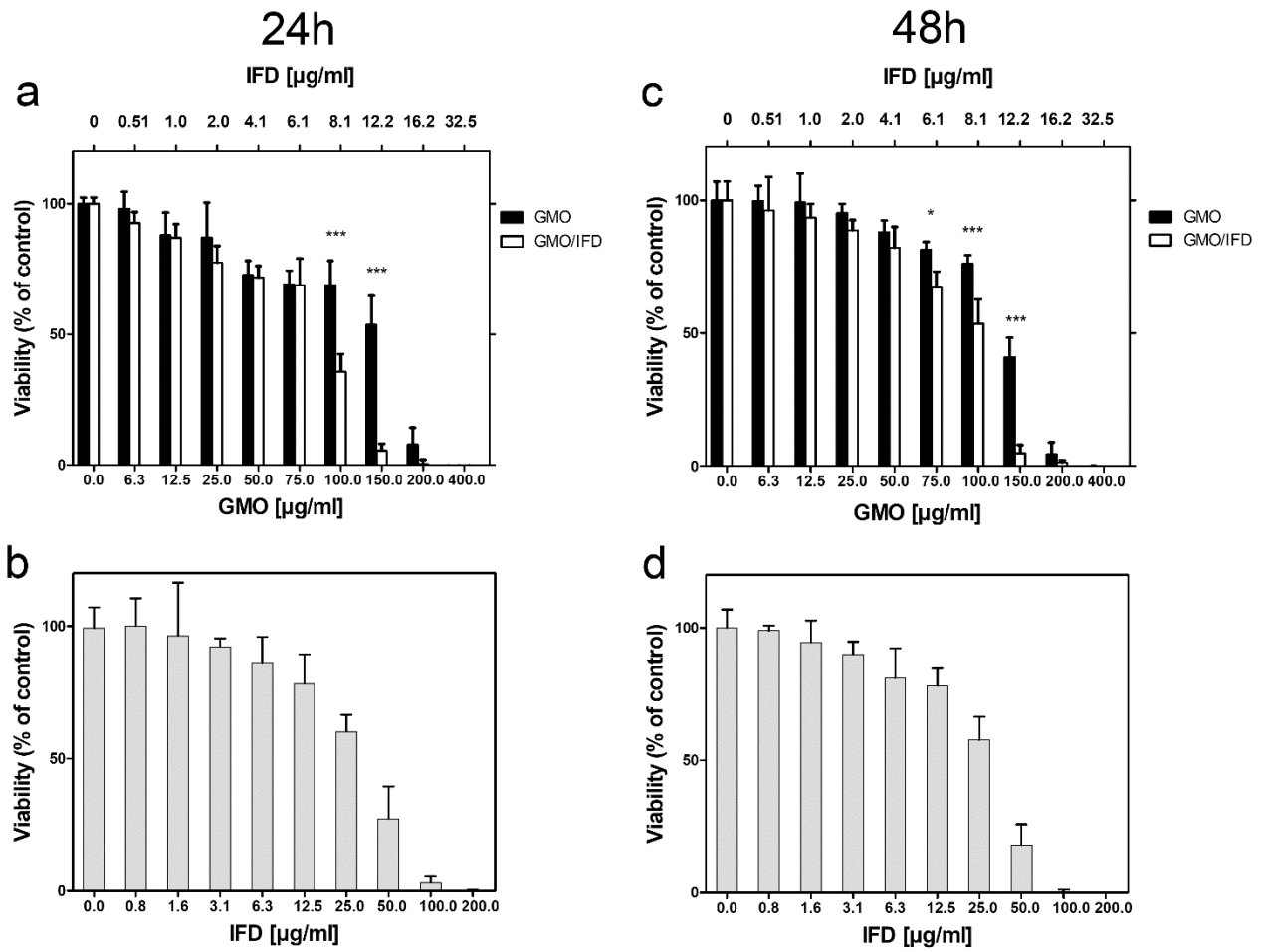

Figure 4. Antiproliferative activity, determined by MTT assay, of IFD, GMO, and GMO/IFD on MDA-MB 231 cells culture. Cells were treated with various concentration of GMO/IFD and GMO, for 24 (a) and 48 h (c). IFD concentrations for each formulation are reported above each panel. Antiproliferative activity of IFD was tested (b, d). Values are mean ± SD, n = 3. The significance of differences between the effect of free and encapsulated FD is indicated by dots above the compared columns (*$p < 0.05$; **$p < 0.01$; ***$p < 0.001$).

Combination Index (CI) analysis was performed using CompuSyn software to valuate if the combination of GMO and IFD has additive or synergistic effect, as given by the CI value: a combination index < 1 indicates synergism, a value of 1 indicates additivity and a value > 1 indicates antagonism.

The dose-response effects of IFD, GMO and GMO/IFD at 24 and 48 h were determined by using concentrations of 0.78, 1.56, 3.125, 6.25, 12.5, 25, 50, 100 and 200 µg/mL and 6.3, 12.5, 25, 50, 75, 100, 150, 200 and 400 for IFD and GMO, respectively and are shown in Figure 5(a). A constant ratio (1.625:20) was used to establish the doses used in combinatory treatment groups and to determine the CI values. IFD and GMO exhibited a synergistic effect in the studied cellular line (Figure 5(b)) as indicated by the CI values <1. The synergism was reduced after 48 h of incubation.

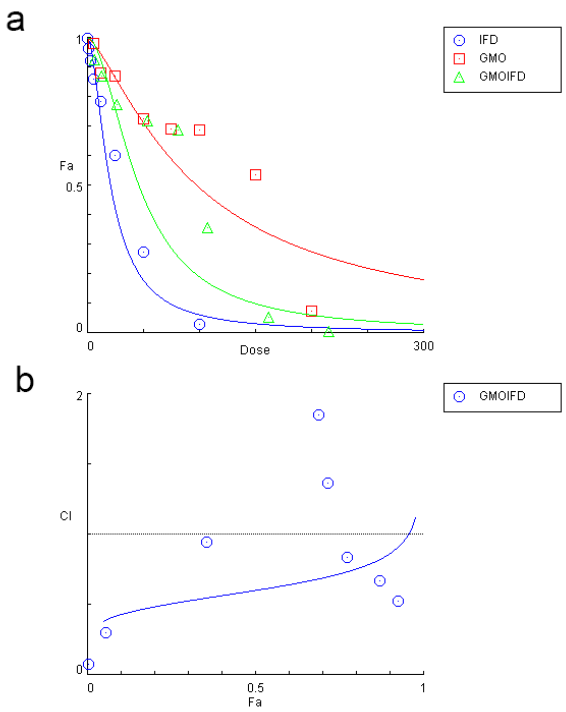

Figure 5. CompuSyn analysis of cytotoxicity data was used to determine synergism, additivity and antagonism between IFD and GMO in MDA-MB 231 cells incubated for 24 h. (a) Dose-effect plots of IFD, GMO and GMO/IFD. (b) CI plots: CI values <1 indicate synergism between IFD and GMO. CI, combination index; Fa, fraction affected.

4. Conclusions

In this work, we exploit the possibility to encapsulate the lipophilic molecule IFD in liquid crystalline nanostructures with the purpose of enhancing its stability and biological activity. The IFD-loaded bulk phases were characterized by SAXS and UVRR and it was found that IFD encapsulation induced a transition from the *Im3m* cubic to the inversed hexagonal phase and significant shifts in the components of IFD Raman spectrum, both confirming its presence in the hydrophobic compartment of the matrix. IFD-loaded nanoparticles had a small size and narrow size distribution with a high entrapment efficiency thanks to their unique property of incorporation of hydrophobic drugs in their internal domains. *In vitro*, these nanoparticles were found to better inhibit breast cancer MDA-MB 231 cells proliferation when compared to free IFD and this improvement could be due to the synergism between IFD and GMO hexosomes, likely because of differences in the internalization process. Further studies are already in progress to clarify this point. The results obtained in this work

confirm that hexosomes are promising and useful vehicles for the delivery of hydrophobic anticancer agents.

Acknowledgment

We thank CERIC-ERIC Consortium for the access to experimental facilities and financial support.

References

(1) Newman, D. J.; Cragg, G. M. Natural Products as Sources of New Drugs over the Last 25 Years ⊥. *J. Nat. Prod.* **2007**, *70* (3), 461–477. https://doi.org/10.1021/np068054v.
(2) Karimi, A.; Majlesi, M.; Rafieian-Kopaei, M. Herbal versus Synthetic Drugs; Beliefs and Facts. 4.
(3) Ozaslan, M.; Oguzkan, S. B. Use of Plant Extracts in Alternative Medicine. *Pak. J. Biol. Sci.* **2018**, *21* (1), 1–7. https://doi.org/10.3923/pjbs.2018.1.7.
(4) Schmidt, B. M. Responsible Use of Medicinal Plants for Cosmetics. *HortScience* **2012**, *47* (8), 985–991. https://doi.org/10.21273/HORTSCI.47.8.985.
(5) Chemat, F.; Vian, M. A.; Cravotto, G. Green Extraction of Natural Products: Concept and Principles. *Int. J. Mol. Sci.* **2012**, *13* (7), 8615–8627. https://doi.org/10.3390/ijms13078615.
(6) Altemimi, A.; Lakhssassi, N.; Baharlouei, A.; Watson, D. G.; Lightfoot, D. A. Phytochemicals: Extraction, Isolation, and Identification of Bioactive Compounds from Plant Extracts. *Plants* **2017**, *6* (4), 42. https://doi.org/10.3390/plants6040042.
(7) Dekebo, A.; Dagne, E.; Sterner, O. Furanosesquiterpenes from Commiphora Sphaerocarpa and Related Adulterants of True Myrrh. *Fitoterapia* **2002**, *73* (1), 48–55. https://doi.org/10.1016/S0367-326X(01)00367-7.
(8) Sun, X.-Y.; Zheng, Y.-P.; Lin, D.-H.; Zhang, H.; Zhao, F.; Yuan, C.-S. Potential Anti-Cancer Activities of Furanodiene, A Sesquiterpene from Curcuma Wenyujin. *Am. J. Chin. Med.* **2009**, *37* (03), 589–596. https://doi.org/10.1142/S0192415X09007077.
(9) Weyerstahl, P.; Marschall-Weyerstahl, H.; Christiansen, C.; Oguntimein, B. O.; Adeoye, A. O. Volatile Constituents of Eugenia Uniflora Leaf Oil1. *Planta Med.* **1988**, *54* (6), 546–549. https://doi.org/10.1055/s-2006-962544.
(10) Maggi, F.; Barboni, L.; Papa, F.; Caprioli, G.; Ricciutelli, M.; Sagratini, G.; Vittori, S. A Forgotten Vegetable (Smyrnium Olusatrum L., Apiaceae) as a Rich Source of Isofuranodiene. *Food Chem.* **2012**, *135* (4), 2852–2862. https://doi.org/10.1016/j.foodchem.2012.07.027.
(11) Maggi, F.; Papa, F.; Giuliani, C.; Maleci Bini, L.; Venditti, A.; Bianco, A.; Nicoletti, M.; Iannarelli, R.; Caprioli, G.; Sagratini, G.; et al. Essential Oil Chemotypification and Secretory Structures of the Neglected Vegetable *Smyrnium Olusatrum* L. (Apiaceae) Growing in Central Italy: Phytochemical Investigation of Smyrnium Olusatrum. *Flavour Fragr. J.* **2015**, *30* (2), 139–159. https://doi.org/10.1002/ffj.3221.
(12) Nair, A.; Amalraj, A.; Jacob, J.; Kunnumakkara, A. B.; Gopi, S. Non-Curcuminoids from Turmeric and Their Potential in Cancer Therapy and Anticancer Drug Delivery Formulations. *Biomolecules* **2019**, *9* (1), 13. https://doi.org/10.3390/biom9010013.
(13) Quassinti, L.; Maggi, F.; Barboni, L.; Ricciutelli, M.; Cortese, M.; Papa, F.; Garulli, C.; Kalogris, C.; Vittori, S.; Bramucci, M. Wild Celery (Smyrnium Olusatrum L.) Oil and Isofuranodiene Induce Apoptosis in Human Colon Carcinoma Cells. *Fitoterapia* **2014**, *97*, 133–141. https://doi.org/10.1016/j.fitote.2014.06.004.

(14) Quassinti, L.; Bramucci, M.; Lupidi, G.; Barboni, L.; Ricciutelli, M.; Sagratini, G.; Papa, F.; Caprioli, G.; Petrelli, D.; Vitali, L. A.; et al. In Vitro Biological Activity of Essential Oils and Isolated Furanosesquiterpenes from the Neglected Vegetable Smyrnium Olusatrum L. (Apiaceae). *Food Chem.* **2013**, *138* (2–3), 808–813. https://doi.org/10.1016/j.foodchem.2012.11.075.
(15) Brunetti, A.; Marinelli, O.; Morelli, M. B.; Iannarelli, R.; Amantini, C.; Russotti, D.; Santoni, G.; Maggi, F.; Nabissi, M. Isofuranodiene Synergizes with Temozolomide in Inducing Glioma Cells Death. *Phytomedicine* **2019**, *52*, 51–59. https://doi.org/10.1016/j.phymed.2018.09.220.
(16) Petrelli, R.; Ranjbarian, F.; Dall'Acqua, S.; Papa, F.; Iannarelli, R.; Ngahang Kamte, S. L.; Vittori, S.; Benelli, G.; Maggi, F.; Hofer, A.; et al. An Overlooked Horticultural Crop, Smyrnium Olusatrum, as a Potential Source of Compounds Effective against African Trypanosomiasis. *Parasitol. Int.* **2017**, *66* (2), 146–151. https://doi.org/10.1016/j.parint.2017.01.001.
(17) Makabe, H.; Maru, N.; Kuwabara, A.; Kamo, T.; Hirota, M. Anti-Inflammatory Sesquiterpenes from Curcuma Zedoaria. *Nat. Prod. Res.* **2006**, *20* (7), 680–685. https://doi.org/10.1080/14786410500462900.
(18) Matsuda, H.; Ninomiya, K.; Morikawa, T.; Yoshikawa, M. Inhibitory Effect and Action Mechanism of Sesquiterpenes from Zedoariae Rhizoma on D-Galactosamine / Lipopolysaccharide-Induced Liver Injury. *Bioorg. Med. Chem. Lett.* **1998**, *8* (4), 339–344. https://doi.org/10.1016/S0960-894X(98)00021-3.
(19) Xiao, Y.; Feng-Qing, Y.; Shao-Ping, L.; Jian-Li, G.; Guang, H.; Sin-Cheng, L.; Emilia, C. L.; Kwok-Pui, F.; Yi-Tao, W.; Simon, L. M.-Y. Furanodiene Induces G2/M Cell Cycle Arrest and Apoptosis through MAPK Signaling and Mitochondria-Caspase Pathway in Human Hepatocellular Carcinoma Cells. *Cancer Biol. Ther.* **2007**, *6* (7), 1044–1050. https://doi.org/10.4161/cbt.6.7.4317.
(20) Li, W.; Shi, J.; Papa, F.; Maggi, F.; Chen, X. Isofuranodiene, the Main Volatile Constituent of Wild Celery (Smyrnium Olusatrum L.), Protects d-Galactosamin/Lipopolysacchride-Induced Liver Injury in Rats. *Nat. Prod. Res.* **2016**, *30* (10), 1162–1165. https://doi.org/10.1080/14786419.2015.1041139.
(21) Li, Y.-W.; Zhu, G.-Y.; Shen, X.-L.; Chu, J.-H.; Yu, Z.-L.; Fong, W.-F. Furanodienone Induces Cell Cycle Arrest and Apoptosis by Suppressing EGFR/HER2 Signaling in HER2-Overexpressing Human Breast Cancer Cells. *Cancer Chemother. Pharmacol.* **2011**, *68* (5), 1315–1323. https://doi.org/10.1007/s00280-011-1624-x.
(22) Li, Y.-W.; Zhu, G.-Y.; Shen, X.-L.; Chu, J.-H.; Yu, Z.-L.; Fong, W.-F. Furanodienone Inhibits Cell Proliferation and Survival by Suppressing ERα Signaling in Human Breast Cancer MCF-7 Cells. *J. Cell. Biochem.* **2011**, *112* (1), 217–224. https://doi.org/10.1002/jcb.22922.
(23) Ma, E.; Wang, X.; Li, Y.; Sun, X.; Tai, W.; Li, T.; Guo, T. Induction of Apoptosis by Furanodiene in HL60 Leukemia Cells through Activation of TNFR1 Signaling Pathway. *Cancer Lett.* **2008**, *271* (1), 158–166. https://doi.org/10.1016/j.canlet.2008.06.008.
(24) Zhong, Z.-F.; Qiang, W.-A.; Wang, C.-M.; Tan, W.; Wang, Y.-T. Furanodiene Enhances the Anti-Cancer Effects of Doxorubicin on ERα-Negative Breast Cancer Cells in Vitro. *Eur. J. Pharmacol.* **2016**, *774*, 10–19. https://doi.org/10.1016/j.ejphar.2015.11.039.
(25) Maggi, F.; Papa, F.; Pucciarelli, S.; Bramucci, M.; Quassinti, L.; Barboni, L.; Ben, D. D.; Ramadori, A. T.; Graiff, C.; Galassi, R. Stabilization of the Cyclodecadiene Derivative Isofuranodiene by Silver (I) Coordination. Mechanistic and Biological Aspects. *Fitoterapia* **2017**, *117*, 52–60. https://doi.org/10.1016/j.fitote.2016.12.009.
(26) Pavela, R.; Pavoni, L.; Bonacucina, G.; Cespi, M.; Kavallieratos, N. G.; Cappellacci, L.; Petrelli, R.; Maggi, F.; Benelli, G. Rationale for Developing Novel Mosquito Larvicides Based on Isofuranodiene Microemulsions. *J. Pest Sci.* **2019**, *92* (2), 909–921. https://doi.org/10.1007/s10340-018-01076-3.

(27) Zhang, J.; He, Y.; Jiang, J.; Li, M.; Jin, C.; Wang, L.; Wang, D. *In Vitro* and *in Vivo* Evaluation of Folate-Mediated PEGylated Nanostructured Lipid Carriers for the Efficient Delivery of Furanodiene. *Drug Dev. Ind. Pharm.* **2017**, *43* (10), 1610–1618. https://doi.org/10.1080/03639045.2017.1328429.
(28) Gershanik, T.; Benita, S. Self-Dispersing Lipid Formulations for Improving Oral Absorption of Lipophilic Drugs. *Eur. J. Pharm. Biopharm.* **2000**, *50* (1), 179–188. https://doi.org/10.1016/S0939-6411(00)00089-8.
(29) zur Mühlen, A.; Schwarz, C.; Mehnert, W. Solid Lipid Nanoparticles (SLN) for Controlled Drug Delivery – Drug Release and Release Mechanism. *Eur. J. Pharm. Biopharm.* **1998**, *45* (2), 149–155. https://doi.org/10.1016/S0939-6411(97)00150-1.
(30) Li, G.; Lin, D.-H.; Xie, X.-X.; Qin, L.-F.; Wang, J.-T.; Liu, K. Uptake and Transport of Furanodiene in Caco-2 Cell Monolayers: A Comparison Study between Furanodiene and Furanodiene Loaded PLGA Nanoparticles. *Chin. J. Nat. Med.* **2013**, *11* (1), 49–55. https://doi.org/10.1016/S1875-5364(13)60007-2.
(31) Cespi, M.; Quassinti, L.; Perinelli, D. R.; Bramucci, M.; Iannarelli, R.; Papa, F.; Ricciutelli, M.; Bonacucina, G.; Palmieri, G. F.; Maggi, F. Microemulsions Enhance the Shelf-Life and Processability of *Smyrnium Olusatrum* L. Essential Oil: Microemulsions Enhance Shelf-Life and Processability of AEO. *Flavour Fragr. J.* **2017**, *32* (3), 159–164. https://doi.org/10.1002/ffj.3367.
(32) Zhao, Y.; Wang, C.; Chow, A. H. L.; Ren, K.; Gong, T.; Zhang, Z.; Zheng, Y. Self-Nanoemulsifying Drug Delivery System (SNEDDS) for Oral Delivery of Zedoary Essential Oil: Formulation and Bioavailability Studies. *Int. J. Pharm.* **2010**, *383* (1), 170–177. https://doi.org/10.1016/j.ijpharm.2009.08.035.
(33) Mezzenga, R.; Seddon, J.M.; Drummond, C.J.; Boyd, B.J.; Schröder-Turk, G.E.; Sagalowicz, L. Nature-Inspired Design and Application of Lipidic Lyotropic Liquid Crystals *Adv. Mater.* **2019**, *31*, 1900818. https://doi.org/10.1002.adma.20190818.
(34) Seddon, J. M. Structure of the Inverted Hexagonal (HII) Phase, and Non-Lamellar Phase Transitions of Lipids. *Biochim. Biophys. Acta BBA - Rev. Biomembr.* **1990**, *1031* (1), 1–69. https://doi.org/10.1016/0304-4157(90)90002-T.
(35) Garti, N.; Libster, D.; Aserin, A. Lipid Polymorphism in Lyotropic Liquid Crystals for Triggered Release of Bioactives. *Food Funct.* **2012**, *3* (7), 700. https://doi.org/10.1039/c2fo00005a.
(36) Kaasgaard, T.; Drummond, C. J. Ordered 2-D and 3-D Nanostructured Amphiphile Self-Assembly Materials Stable in Excess Solvent. *Phys. Chem. Chem. Phys.* **2006**, *8* (43), 4957. https://doi.org/10.1039/b609510k.
(37) Larsson, K. Aqueous Dispersions of Cubic Lipid–Water Phases. *Curr. Opin. Colloid Interface Sci.* **2000**, *5* (1), 64–69. https://doi.org/10.1016/S1359-0294(00)00040-6.
(38) Barriga, H. M. G.; Holme, M. N.; Stevens, M. M. Cubosomes: The Next Generation of Smart Lipid Nanoparticles? *Angew. Chem. Int. Ed.* **2019**, *58* (10), 2958–2978. https://doi.org/10.1002/anie.201804067.
(39) Angelova, A.; Garamus, V.M.; Angelov, B.; Tian, X.; Li,Y.; Zou, A. Advances in structural design of lipid-based nanoparticle carriers for delivery of macromolecular drugs, phytochemicals and anti-tumor agents *Adv. Colloid Interface Sci.* **2017**, *249*, 331-345. http://dx.doi.org/10.1016/j.cis.2017.04.006
(40) Maiorova, L. A.; Erokhina, S. I.; Pisani, M.; Barucca, G.; Marcaccio, M.; Koifman, O. I.; Salnikov, D. S.; Gromova, O. A.; Astolfi, P.; Ricci, V.; et al. Encapsulation of Vitamin B12 into Nanoengineered Capsules and Soft Matter Nanosystems for Targeted Delivery. *Colloids Surf. B Biointerfaces* **2019**, *182*, 110366. https://doi.org/10.1016/j.colsurfb.2019.110366.
(41) Angelova, A.; Angelov, B.; Mutafchieva, R.; Lesieur, S.; Couvreur, P. Self-Assembled Multicompartment Liquid Crystalline Lipid Carriers for Protein, Peptide, and Nucleic Acid Drug Delivery. *Acc. Chem. Res.* **2011**, *44* (2), 147–156. https://doi.org/10.1021/ar100120v.

(42) Zhai, J.; Fong, C.; Tran, N.; Drummond, C. J. Non-Lamellar Lyotropic Liquid Crystalline Lipid Nanoparticles for the Next Generation of Nanomedicine. *ACS Nano* **2019**, acsnano.8b07961. https://doi.org/10.1021/acsnano.8b07961.
(43) Milak, S.; Zimmer, A. Glycerol Monooleate Liquid Crystalline Phases Used in Drug Delivery Systems. *Int. J. Pharm.* **2015**, *478* (2), 569–587. https://doi.org/10.1016/j.ijpharm.2014.11.072.
(44) Qiu, H.; Caffrey, M. The Phase Diagram of the Monoolein/Water System: Metastability and Equilibrium Aspects. *Biomaterials* **2000**, *21* (3), 223–234. https://doi.org/10.1016/S0142-9612(99)00126-X.
(45) Barauskas, J.; Landh, T. Phase Behavior of the Phytantriol/Water System. *Langmuir* **2003**, *19* (23), 9562–9565. https://doi.org/10.1021/la0350812.
(46) Final Report on the Safety Assessment of Phytantriol1. *Int. J. Toxicol.* **2007**, *26* (1_suppl), 107–114. https://doi.org/10.1080/10915810601163947.
(47) Administration, U. F. A. D. *Food and Drug Administration HHS*; 2008.
(48) Astolfi, P.; Giorgini, E.; Gambini, V.; Rossi, B.; Vaccari, L.; Vita, F.; Francescangeli, O.; Marchini, C.; Pisani, M. Lyotropic Liquid-Crystalline Nanosystems as Drug Delivery Agents for 5-Fluorouracil: Structure and Cytotoxicity. *Langmuir* **2017**, *33* (43), 12369–12378. https://doi.org/10.1021/acs.langmuir.7b03173.
(49) Astolfi, P.; Giorgini, E.; Adamo, F. C.; Vita, F.; Logrippo, S.; Francescangeli, O.; Pisani, M. Effects of a Cationic Surfactant Incorporation in Phytantriol Bulk Cubic Phases and Dispersions Loaded with the Anticancer Drug 5-Fluorouracil. *J. Mol. Liq.* **2019**, *286*, 110954. https://doi.org/10.1016/j.molliq.2019.110954.
(50) Benelli, G.; Pavela, R.; Iannarelli, R.; Petrelli, R.; Cappellacci, L.; Cianfaglione, K.; Afshar, F. H.; Nicoletti, M.; Canale, A.; Maggi, F. Synergized Mixtures of Apiaceae Essential Oils and Related Plant-Borne Compounds: Larvicidal Effectiveness on the Filariasis Vector Culex Quinquefasciatus Say. *Ind. Crops Prod.* **2017**, *96*, 186–195. https://doi.org/10.1016/j.indcrop.2016.11.059.
(51) Benelli, G.; Pavela, R.; Canale, A.; Nicoletti, M.; Petrelli, R.; Cappellacci, L.; Galassi, R.; Maggi, F. Isofuranodiene and Germacrone from Smyrnium Olusatrum Essential Oil as Acaricides and Oviposition Inhibitors against Tetranychus Urticae: Impact of Chemical Stabilization of Isofuranodiene by Interaction with Silver Triflate. *J. Pest Sci.* **2017**, *90* (2), 693–699. https://doi.org/10.1007/s10340-016-0829-5.
(52) D'Amico, F.; Saito, M.; Bencivenga, F.; Marsi, M.; Gessini, A.; Camisasca, G.; Principi, E.; Cucini, R.; Di Fonzo, S.; Battistoni, A.; et al. UV Resonant Raman Scattering Facility at Elettra. *Nucl. Instrum. Methods Phys. Res. Sect. Accel. Spectrometers Detect. Assoc. Equip.* **2013**, *703*, 33–37. https://doi.org/10.1016/j.nima.2012.11.037.
(53) Frisch, M. J.; Trucks, G. W.; Schlegel, H. B.; Scuseria, G. E.; Robb, M. A.; Cheeseman, J. R.; Scalmani, G.; Barone, V.; Mennucci, B.; Petersson, G. A.; et al. *Gaussian 09, Revision D.01*; Gaussian, Inc.: Wallingford CT, 2013.
(54) Perdew, J. P.; Burke, K.; Ernzerhof, M. Generalized Gradient Approximation Made Simple. *Phys. Rev. Lett.* **1996**, *77* (18), 3865–3868. https://doi.org/10.1103/PhysRevLett.77.3865.
(55) Grimme, S.; Ehrlich, S.; Goerigk, L. Effect of the Damping Function in Dispersion Corrected Density Functional Theory. *J. Comput. Chem.* **2011**, *32* (7), 1456–1465. https://doi.org/10.1002/jcc.21759.
(56) Quassinti, L.; Lupidi, G.; Maggi, F.; Sagratini, G.; Papa, F.; Vittori, S.; Bianco, A.; Bramucci, M. Antioxidant and Antiproliferative Activity of *Hypericum Hircinum* L. Subsp. *Majus* (Aiton) N. Robson Essential Oil. *Nat. Prod. Res.* **2013**, *27* (10), 862–868. https://doi.org/10.1080/14786419.2012.677044.
(57) Chou, T.-C.; Martin N. *CompuSyn for Drug Combinations: PC Software and User's Guide: A Computer Program for Quantitation of Synergism and Antagonism in Drug Combinations,*

and the Determination of IC50 and ED50 and LD50 Values.; ComboSyn Inc: Paramus NJ, 2005.

(58) Nakano, M,; Sugita, A.; Matsuoka, H,; Handa, T. Small-Angle X-ray Scattering and 13C NMR Investigation on the Internal Structure of "Cubosomes". *Langmuir*. **2001**, *17*, 3917-3922. htpps:// doi.org/10.1021/la010224a

(59) Falchi, A.M.; Rosa, A.; Atzeri, A.; Incani, A.; Lampis, S.; Meli, V.; Caltagirone, C.; Murgia, S. *Toxicol. Res.* **2015**, *4*, 1025-1036. https://doi.org/ 10.1039/c5tx00078e

(60) Fong, C.; Le, T.; Drummond, C.J. *Chem. Soc. Rev.* **2012**, *41*, 1297-1322. https://doi.org/ 10.1039/c1cs15148g

(61) Rizwan, S. B.; Assmus, D.; Boehnke, A.; Hanley, T.; Boyd, B. J.; Rades, T.; Hook, S. Preparation of Phytantriol Cubosomes by Solvent Precursor Dilution for the Delivery of Protein Vaccines. *Eur. J. Pharm. Biopharm.* **2011**, *79* (1), 15–22. https://doi.org/10.1016/j.ejpb.2010.12.034.

(62) Svensson, O.; Thuresson, K.; Arnebrant, T. Interactions between Drug Delivery Particles and Mucin in Solution and at Interfaces. *Langmuir* **2008**, *24* (6), 2573–2579. https://doi.org/10.1021/la702680x.

(63) Marinova, K. G.; Alargova, R. G.; Denkov, N. D.; Velev, O. D.; Petsev, D. N.; Ivanov, I. B.; Borwankar, R. P. Charging of Oil−Water Interfaces Due to Spontaneous Adsorption of Hydroxyl Ions. *Langmuir* **1996**, *12* (8), 2045–2051. https://doi.org/10.1021/la950928i.

(64) Chountoulesi, M.; Pippa, N.; Pispas, S.; Chrysina, E. D.; Forys, A.; Trzebicka, B.; Demetzos, C. Cubic Lyotropic Liquid Crystals as Drug Delivery Carriers: Physicochemical and Morphological Studies. *Int. J. Pharm.* **2018**, *550* (1–2), 57–70. https://doi.org/10.1016/j.ijpharm.2018.08.003.

(65) Zhong, Z.; Dang, Y.; Yuan, X.; Guo, W.; Li, Y.; Tan, W.; Cui, J.; Lu, J.; Zhang, Q.; Chen, X.; et al. Furanodiene, a Natural Product, Inhibits Breast Cancer Growth Both ***in Vitro*** and ***in Vivo*** . *Cell. Physiol. Biochem.* **2012**, *30* (3), 778–790. https://doi.org/10.1159/000341457.

(66) Buccioni, M.; Dal Ben, D.; Lambertucci, C.; Maggi, F.; Papa, F.; Thomas, A.; Santinelli, C.; Marucci, G. Antiproliferative Evaluation of Isofuranodiene on Breast and Prostate Cancer Cell Lines. *Sci. World J.* **2014**, *2014*, 1–6. https://doi.org/10.1155/2014/264829.

(67) Hinton, T. M.; Grusche, F.; Acharya, D.; Shukla, R.; Bansal, V.; Waddington, L. J.; Monaghan, P.; Muir, B. W. Bicontinuous Cubic Phase Nanoparticle Lipid Chemistry Affects Toxicity in Cultured Cells. *Toxicol Res* **2014**, *3* (1), 11–22. https://doi.org/10.1039/C3TX50075F.

(68) Rakotoarisoa, M.; Angelov, B.; Garamus, V. M.; Angelova, A. Curcumin- and Fish Oil-Loaded Spongosome and Cubosome Nanoparticles with Neuroprotective Potential against H2O2-Induced Oxidative Stress in Differentiated Human SH-SY5Y Cells. *ACS Omega* **2019**, 13.

(69) Tran, N. Nanostructure and Cytotoxicity of Self-Assembled Monoolein–Capric Acid Lyotropic Liquid Crystalline Nanoparticles. *RSC Adv.* **2015**, 11.

(70) Zhai, J.; Luwor, R. B.; Ahmed, N.; Escalona, R.; Tan, F. H.; Fong, C.; Ratcliffe, J.; Scoble, J. A.; Drummond, C. J.; Tran, N. Paclitaxel-Loaded Self-Assembled Lipid Nanoparticles as Targeted Drug Delivery Systems for the Treatment of Aggressive Ovarian Cancer. *ACS Appl Mater Interfaces* **2018**, 12.

(71) Rarokar, N. R.; Khedekar, P. B.; Bharne, A. P.; Umekar, M. J. Development of Self-Assembled Nanocarriers to Enhance Antitumor Efficacy of Docetaxel Trihydrate in MDA-MB-231 Cell Line. *Int. J. Biol. Macromol.* **2019**, *125*, 1056–1068. https://doi.org/10.1016/j.ijbiomac.2018.12.130.

(72) Freag, M. S.; Elnaggar, Y. S.; Abdelmonsif, D. A.; Abdallah, O. Y. Layer-by-Layer-Coated Lyotropic Liquid Crystalline Nanoparticles for Active Tumor Targeting of Rapamycin. *Nanomed.* **2016**, *11* (22), 2975–2996. https://doi.org/10.2217/nnm-2016-0236.

(73) Tran, N.; Mulet, X.; Hawley, A. M.; Hinton, T. M.; Mudie, S. T.; Muir, B. W.; Giakoumatos, E. C.; Waddington, L. J.; Kirby, N. M.; Drummond, C. J. Nanostructure and Cytotoxicity of Self-Assembled Monoolein–Capric Acid Lyotropic Liquid Crystalline Nanoparticles. *RSC Adv.* **2015**, *5* (34), 26785–26795. https://doi.org/10.1039/C5RA02604K.
(74) Mezzenga, R.; Meyer, C.; Servais, C.; Romoscanu, A. I.; Sagalowicz, L.; Hayward, R. C. Shear Rheology of Lyotropic Liquid Crystals: A Case Study. *Langmuir* **2005**, *21* (8), 3322–3333. https://doi.org/10.1021/la046964b.
(75) Tilley, A. J.; Drummond, C. J.; Boyd, B. J. Disposition and Association of the Steric Stabilizer Pluronic® F127 in Lyotropic Liquid Crystalline Nanostructured Particle Dispersions. *J. Colloid Interface Sci.* **2013**, *392*, 288–296. https://doi.org/10.1016/j.jcis.2012.09.051.